A New Family of Molecular Metals Based on Bis(ethylenethio)tetrathiafulvalene (BET-TTF) and Octahedral Counterions

Judit Tarrés, Núria Santaló, Montse Mas, Elies Molins, Jaume Veciana, and Concepció Rovira*

Institut de Ciència de Materials de Barcelona (CSIC), Campus de la U.A.B., 08193 Bellaterra, Spain

Syaulan Yang, Haeseong Lee, and Dwaine O. Cowan

Department of Chemistry, The Johns Hopkins University, Baltimore, Maryland 21218

Marie-Liesse Doublet and Enric Canadell

Laboratoire de Chimie Théorique (CNRS URA 506), Université Paris-Sud, 91405 Orsay, France

Received March 20, 1995[⊗]

The electrochemical synthesis and physical characterization of a series of new bis(ethylenethio)tetrathiafulvalene (BET-TTF) based salts, (BET-TTF)PF_6, and (BET-TTF)$_2$X (X = PF_6, AsF_6, and SbF_6), are reported. In all X-ray crystal structures, only the *E* isomer of BET-TTF is present. The (BET-TTF)PF_6 (**2**) salt crystallizes in the centrosymmetric group *P*21/*a*, in which donors stack uniformly along the *b* crystallographic axis in a herringbone pattern with a crystal packing similar to α-phases of BEDT-TTF. The three 2:1 salts crystallize in the triclinic *P*−1 space group and are isostructural, being the crystal packing motif very similar to the β-phases of BEDT-TTF. In salts (BET-TTF)$_2AsF_6$ (**4**) and (BET-TTF)$_2SbF_6$ (**5**) a structural disorder due to the external sulfur positions of BET-TTF is observed. Band electronic calculations on these structures indicate a quasi-2D electronic character for salts **4** and **5**. All 2:1 salts show metallic character down to ~100 K, where a very broad transition toward an activated conductivity is observed. The relationships between the crystal structures, physical properties, and electronic structures are discussed.

Introduction

The search for new organic superconductors has mainly focused on BEDT-TTF derivatives[1] since ambient-pressure bulk superconductivity (T_c ~ 1.5 K) was discovered in (BEDT-TTF)$_2I_3$.[2] To date, the κ-phase (BEDT-TTF)$_2$[Cu{N(CN)$_2$}][Cl] exhibits the highest critical temperature T_c (12.8 K, 0.3 kbar) of any heterocyclic molecular superconductor.[3]

In addition, some other multichalcogen electron donors and acceptors as MDT-TTF,[4] DMET-TTF,[5] and Ni(dmit)$_2$[6] have also been used for the preparation of molecular superconductors.

Although there are significant crystal-structure packing differences among the various superconductors, a common feature is the presence of an extensive network of intermolecular S···S interactions that gives rise to two-dimensional (2D) metallic character.[1] The outer sulfur atoms of the donors and acceptor play an essential role in this enhancement of the dimensionality. In the search for new electron-donor molecules to produce organic superconductors with even higher T_c's, an appealing approach is to change the number and position of outer sulfur atoms as well as the size of the cyclic substituents of the TTF skeleton. In this way novel structural and electronic features of their salts could be achieved tuning the physical properties. We are involved in the synthesis of new multisulfur π-electron donors having one sulfur atom placed in different positions of the outer five member cyclic substituents of the TTF core[7] and in the preparation and study of

[⊗] Abstract published in *Advance ACS Abstracts,* July 1, 1995.

(1) (a) *The Physics and Chemistry of Organic Superconductors;* Saito, G., Kagoshima, S., Eds.; Springer-Verlag: Berlin, 1990. (b) *Organic Superconductors;* Williams, J. M., Ferraro, J. R., Thorn, R. J., Carlson, K. D., Geiser, U., Wang, H. H., Kini, A. M., Whangbo, M.-H., Eds.; Prentice Hall: Englewood Cliffs, NJ, 1992.

(2) . (a) Yagubskii, E. B.; Shegolev, I. F.; Laukhin, V. N.; Konovich, P. A.; Kartsovnik, M. W.; Zvarykina, A. V.; Buravov, L. I. *JEPT Lett.* **1984**, *39*, 12. (b) Williams, J. M.; Emge, T. J.; Wang, H. H.; Beno, M. A.; Copps, P.; T.; Hall, L. N.; Carlson, K. D.; Crabtree, G. W. *Inorg. Chem.* **1984**, *23*, 2558.

(3) Williams, J. M.; Kini, A. M.; Wang, H. H.; Carlson, K. D.; Geiser, U.; Montgomery, L. K.; Pyrka, G. J.; Watkins, D. M.; Kommers, J. M.; Boryschuk, S. J.; Srieby Crouch, A. V.; Kwok, W. K.; Schirber, J. E.; Overmyer, D. L.; Jung, D.; Whangbo, M.-H. *Inorg. Chem.* **1990**, *29*, 3272.

(4) Papavassiliou, G. C.; Mousdis, G. A.; Zambounis, J. S.; Terzis, A.; Hountas, A.; Hilti, B.; Mayer, C. W.; Pfeiffer, J. *Synth. Met.* **1988**, *B27*, 379.

(5) Kikuchi, K.; Murata, K.; Honda, Y.; Tamiki, T.; Saito, K.; Anzai, H.; Kobayashi, K.; Ishiguro T.; Ikemoto, I. *J. Phys. Soc. Jpn.* **1987**, *56*, 4241.

(6) (a) Kajita, K.; Nishio. Y.; Moriyama, S.; Kato, R.; Kobayashi, H.; Sasaki, W. *Solid State Commun.* **1988**, *65*, 361. (b) Brossard, M.; Ribault, M.; Valade, L.; Cassoux, P. *Physica B & C (Amsterdam)* **1986**, *143*, 378.

(7) (a) Rovira, C.; Santaló N.; Veciana, J. *Tetrahedron Lett.* **1989**, *30*, 7249. (b) Rovira, C.; Santaló N.; Veciana, J.; Claret, J.; Molins E.; Miravitlles, C. *Synth. Met.* **1991**, *41−43*, 2205. (c) Rovira, C.; Veciana, J.; Santaló, N.; Tarrés, J.; Cirujeda, J.; Molins, E. Llorca, J.; Espinosa, E. *J. Org. Chem.* **1994**, *59*, 3307.

0897-4756/95/2807-1558$09.00/0

Table 1. Electrocrystallization Syntheses of the (BET-TTF)$_n$X Salts

	compd				
	(BET-TTF)$_3$PF$_6$·C$_6$H$_5$Cl (**1**)	(BET-TTF)PF$_6$ (**2**)	(BET-TTF)$_2$PF$_6$ (**3**)	(BET-TTF)$_2$AsF$_6$ (**4**)	(BET-TTF)$_2$SbF$_6$ (**5**)
solvent[a]	C$_6$H$_5$Cl	THF	THF	THF or C$_6$H$_5$Cl	C$_6$H$_5$Cl
V, V	3	1.6	1.8	1.8	1.8
J, μA cm^{-2}	1.6–1.9	1.6–2.1	1.6–3.1	1.6–3.7	1.6–2.3
I, μA			0.5	0.7	0.4
J, μA cm^{-2}			1.6	2.2	1.25
donor, mM	1.1×10^{-2}	0.9×10^{-2}	1.1×10^{-2}	1.1×10^{-2}	1.0×10^{-2}
anion, mM	8.6×10^{-2}	8.6×10^{-2}	8.6×10^{-2}	8.6×10^{-2}	8.6×10^{-2}
time, days	5	4	4	4	5

[a] 13 mL of solvent was used in all cases.

their charge-transfer salts with inorganic counterions of different geometries.[8]

In the present study we describe the syntheses, crystal structures, selected physical properties, and band electronic structures of three 2:1 and one 1:1 radical-cation salts of a bis(ethylenethio)tetrathiafulvalene (BET-TTF) donor with octahedral counterions. The BET-TTF donor is of particular interest since it has sulfur atoms placed at the same position than those of BEDT-TTF and also ethylene groups in the cyclic substituent. It is known that those elements have an important contribution to the crystal structures and properties of the BEDT-TTF salts. The size of the cyclic substituent in BET-TTF is smaller than in BEDT-TTF, and for this reason, the conformations of ethylene groups are more restricted. Consequently, we will be able to study how this fact influences in the structural and electronic properties of its derivatives.

Experimental Section

Sample Preparation. BET-TTF was synthesized as previously described[7c] and purified by recrystallization in chlorobenzene. BET-TTF cation radical salts were grown, under anaerobic conditions, at platinum wire electrodes (0.5 mm diameter) in an H-shaped electrocrystallization cell[9] under potentiostatic or galvanostatic conditions using the corresponding tetrabutylammonium salts. All solvents were dried over activated alumina just before use. Crystals obtained in all cases were very thin, and the experimental conditions significantly affect the shape and composition of the crystals; in some cases two salts with different stoichiometries grow in the same electrocrysyallization. The best electrocrystallization conditions for compounds **1**–**5** are summarized in Table 1. The stoichiometries were determined by X-ray crystal structure analysis and/or elemental analysis. Anal. Calcd (obsd) for **1**, $C_{30}H_{24}F_6PS_{18}$·C_6H_5Cl: C, 35.48 (34.70); H, 2.41 (2.32); S, 47.32 (47.24). Anal. Calcd (obsd) for **3**, $C_{20}H_{16}F_6PS_{12}$: C, 30.67 (30.91); H, 2.01 (2.22); S, 48.92 (49.14). Anal. Calcd (obsd) for **4**, $C_{20}H_{16}F_6AsS_{12}$: C, 28.95 (28.81); H, 1.93 (2.12); S, 46.32 (46.13). Anal. Calcd (obsd) for **5**, $C_{20}H_{16}F_6SbS_{12}$: C, 27.39 (27.51); H, 1.83 (2.01); S, 43.82 (43.69).

X-ray Crystal Structure Analysis.[10] Single-crystal diffraction data were collected at room temperature (294 K) on an Enraf-Nonius CAD4 diffractometer equipped with graphite monochromator and Mo Kα radiation (λ = 0.710 73 Å). Unit-cell parameters were determined from a least-squares analysis of 25 reflections. In the (BET-TTF)$_2$PF$_6$ case, it just has been possible to measure the cell parameters due to the low crystal quality. Intensity data were collected by the ω–2θ scan technique and up to $2\theta = 50°$. In all cases L_p corrections were applied and in (BET-TTF)$_2$SbF$_6$ DIFABS[11] absorption correction was done. Due to the plate shape of the (BET-TTF)$_2$AsF$_6$ and the (BET-TTF)PF$_6$ crystals and to minimize the absorption effects, the data were collected using the FLAT PSI mode. This means that the crystal is placed at its minimum absorption position, assuming that it is an infinite flat crystal with negligible thickness.

The (BET-TTF)$_2$SbF$_6$ structure was solved by direct methods with a straigtforward run of the MULTAN 11/84 program,[12] and that of (BET-TTF)$_2$AsF$_6$ was solved by isomorphism to the previous one. The (BET-TTF)PF$_6$ structure was solved by Patterson search methods with a run of the ROTSEARCH program[13] using the DMET coordinates[14] as a model. In all cases full-matrix least-squares refinement was carried out with SHELX76 program,[15] using anisotropic thermal parameters for the non-H atoms and one global isotropic temperature factor for the H atoms.

Conductivity Measurements. Crystal samples with dimensions of 0.50–4.50 mm × 0.02–0.64 mm × 0.02–0.30 mm were mounted with four probes on PC boards with 12.7 μm gold wire. To avoid wire stress to the contacts, small kinks in the wires were made. DuPont 4929 silver paste was mixed with 2-butoxyethyl acetate as a thinner for mounting contacts. The PC board was then attached onto a sample holder which was placed inside of a quasi-isothermal copper can in a constant flow cryostat. A LakeShore Cryotonics DRC82C temperature controller was connected to the sample holder and the copper can to maintain a constant rate of 0.5 °C/min temperature change. A Keithley 220 programmable current source was installed for supplying current to the samples. The current was reversed, and the voltage readings were averaged to remove any extraneous values. Voltage measurements were made with a Keithley 181 nanovoltmeter for metallic samples and a Keithley 619 electrometer for semiconducting samples. The data was collected every 0.05 °C from room temperature down to liquid helium temperatures for a metallic sample and liquid nitrogen temperatures for a semiconducting sample. All of the temperature change, current supply, voltage measurement, and data collection were automatically controlled and managed by a HP9816A computer/HP9121D disk drive.

Thermoelectric Power. Crystal samples with dimensions of 1.2–1.5 mm × 0.1–0.3 mm × 0.01–0.02 mm were mounted

(8) (a) Rovira, C.; Santaló, N.; Veciana J.; Molins E.; Miravitlles, C. *Synth. Met.* **1991**, *41–43*, 2199. (b) Molins, E.; Llorca, J.; Santaló, N.; Veciana, J.; Rovira, C.; Miravitlles, C. *Synth. Met.* **1993**, *55–57*, 1994. (c) Rovira, C.; Veciana, J.; Tarrés, J.; Santaló, N. In *New Organic Materials*; Seoane, C., Martin, N., Eds.; Universidad Complutense Madrid, 1994; p 58. (d) Rovira, C.; Veciana, J.; Tarrés, J.; Molins, E.; Mas, M.; Cowan, D. O.; Yang, S.; Lee, H. *Synth. Met.* **1995**, *70*, 883.

(9) (a) Lee, M. M.; Stokes, J. M.; Wiygul, F. M.; Kistenmacher, T. J.; Cowan, D. O.; Poehler, T. O.; Bloch, A. N.; Fuller, W. W.; Gubser, D. U. *Mol. Cryst. Liq. Cryst.* **1982**, *79*, 145. (b) Engler, E. M.; Greene, R.; Haen, P.; Tomkiewicz, Y.; Mortensen, K.; Berendzen, J. *Mol. Cryst. Liq. Cryst.* **1982**, *79*, 15.

(10) The authors have deposited atomic coordinates for these structures with the Cambridge Crystallographic Data Centre. The coordinates can be obtained, on request, from the Director, Cambridge Crystallographic Data Centre, 12 Union Road, Cambridge, CB2, 1EZ, UK.

(11) Walker, N.; Stuart, D. *Acta Crystallogr.* **1983**, *A39*, 159.

(12) Main, P.; Germain, G.; Woolfson, M. M. *Multan 11/84, "A System of Computer Programs for the Automatic Solution of Crystal Structures for X-ray Diffraction Data;* University of York (England) and Lovain (Belgium), 1984.

(13) Rius, J.; Miravitlles, C. *ROTSEARCH program for finding molecular orientations. Acta Crystallogr.* **1987**, *A43*, Suppl. 17.2.

(14) Saito, K.; Ishikawa, Y.; Kikuchi, K.; Ikemoto, I.; Kobayashi, K. *Acta Crystallogr.* **1989**, *C45*, 1403.

(15) Sheldrick, G. M. *Shelx76, Program for Crystal Structure Determination*; University of Cambridge: England, 1976.

Chart 1

(*E*)-BET-TTF (*Z*)-BET-TTF

with 25.4 μm pure gold wires (99.99%, California Fine Wire Co.) and DuPont 4929 silver paste onto a thermoelectric power device. A Keithley 220 current source supplied with ~1 mA current to the heater of the device which made the temperature difference between both ends of the sample to be ~1 K. The thermocouple was made with gold and chromel wires. Readings of the voltage from the thermocouple were monitored by a Hewlett-Packard 3497A microvoltmeter. A Keithley 181 nanovoltmeter was operated to measure the thermoelectric voltage of the sample. The temperature controlling throughout the experiment was performed with a LakeShore Cryotonics DRC 82C temperature controller. The data collection for the experiment was done by a HP9816A computer/HP9121D disk drive from room temperature down to liquid-helium temperature.

ESR measurements were carried out on a Bruker 300E and Varian X-band equipped with an Oxford variable-temperature accessory spectrometers. The modulation amplitude was kept well below the line width, and the microwave power was well below saturation. Variable-temperature experiments carried out on single crystals were performed with the static magnetic field perpendicular to the 001 face of the crystals.

Spectrooptical Characterizations. Transmission measurements of finely ground KBr pellet samples with a weight concentration about 1% have already been carried out using a Nicolet MX1 interferometer (350−4800 cm^{-1} and a UV−visible−NIR Perkin-Elmer 350 spectometer (3850−25000 cm^{-1}).

Band Structure Calculations. The tight-binding band structure calculations[16] were of the extended Hückel type.[17] A modified Wolfsberg−Helmholz formula was used to calculate the nondiagonal $H_{\mu\nu}$ values.[18] Double-ζ orbitals[19] for C and S were used. The exponents (ζ_μ and ζ_μ'), weighting coefficients (c_μ and c_μ') of the double-ζ orbitals, and $H_{\mu\mu}$ (eV) values used were 1.831, 1.153, 0.7616, 0.2630, and −21.4 for C 2s; 2.730, 1.257, 0.2595, 0.8025, and −11.4 for C 2p; 2.662, 1.688, 0.5564, 0.4874, and −20.0 for S 3s; and 2.328, 1.333, 0.5208, 0.5439, and −13.3 for S 3p.

Results and Discussion

Crystal Structures. In all the studied salts, only one of the two possible isomers of BET-TTF (Chart 1), the *E* isomer, is present, as occurs in the crystalline neutral donor[7c] and in the (BET-TTF)$AuBr_2$ salt.[8d] The molecular structures of compounds **2** and **5** are shown in Figure 1 together with their atomic numbering schemes. In all salts the TTF moiety of the BET-TTF molecules is planar with the mean plane of the external rings being only slightly distorted as was also observed in neutral BET-TTF.[7c] As expected, the external five membered rings are almost planar, with very small deviation of only one CH_2 group (envelope form) or two CH_2 groups in a half-chair form. Due to the small value of the deviations it is not possible to assign strictly different conformations to these forms.

The three 2:1 salts $(BET\text{-}TTF)_2X$ (**3**, X = PF_6; **4**, X = AsF_6; **5**, X = SbF_6) crystallize in the triclinic $P\bar{1}$ space group and are isoestructural. As expected, an increase in the cell volume is observed with the increase of the anion size (Table 2). In salts **4** and **5** a structural disorder due to the external sulfur positions of BET-TTF is observed. The crystal packing motif is very similar to the β-phases of BEDT-TTF.[1b] The structure consists of alternating sheets of radical cations and anions along the *c* direction. BET-TTF molecules are stacked along the crystallographic *b* axis in a zigzag mode and within the stacks adjacent molecules exhibit the commonly observed ring-over-bond overlap arrangement (Figure 2) being slightly dimerized. The molecular planes of the donor molecules alternate at separations of 3.55 and 3.62 Å in salt **4** and of 3.60 and 3.63 Å in salt **5**. Intermolecular S···S contacts shorter than the sum of the van der Waals radii[20] occur between the stacks involving sulfur atoms of the fulvalenic moiety an those of external rings, as shown in Figure 3. Short F···H contacts between CH_2 groups of BET-TTF and anions are also found being more numerous in $(BET\text{-}TTF)_2SbF_6$ salt, which is the compound that has the biggest anion in the series.

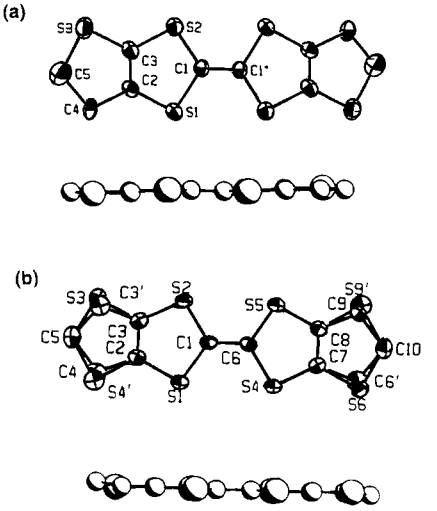

Figure 1. BET-TTF molecules (top and side views) in (b) $(BET\text{-}TTF)_2SbF_6$ and (a) $(BET\text{-}TTF)PF_6$ salts.

The $(BET\text{-}TTF)PF_6$ (**2**) salt crystallizes in the centrosymmetric group $P2_1/a$. Molecules of BET-TTF stack uniformly along the *b* crystallographic axis in a herringbone pattern alternating with stacks of anions (Figure 4). In each donor stack, molecules slip in the direction perpendicular to the central C=C bond instead of slipping along the C=C bond as found in the above described 2:1 salts. The crystal packing motif is very similar to the α-phases of BEDT-TTF.[1b] Only intercolumn (side-by-side) S···S contacts are observed forming a two dimensional network of donors in the *ab* plane. Donor-anion contacts are also established between CH_2 and F groups (Figure 5).

Electronic and Vibrational Spectra. In the electronic spectra of the three 2:1 salts (**3**−**5**) shown in Figure 6, two intense, homogeneous charge-transfer bands are observed. Following the notation of Torrance et al.,[21] the lower frequency bands correspond to the charge-transfer A peak characteristic of a mixed-valence state and are centered at 3200 cm^{-1} for the three salts,

(16) Whangbo, M.-H.; Hoffmann, R. *J. Am. Chem. Soc.* **1978**, *100*, 6093.
(17) Hoffmann, R. *J. Chem. Phys.* **1963**, *39*, 1397.
(18) Ammeter, J. H.; Bürgi, H.-B.; Thibeault, J.; Hoffmann, R. *J. Am. Chem. Soc.* **1978**, *100*, 3686.
(19) (a) Whangbo, M.-H. ; Williams, J. M.; Leung, P. C. W.; Beno, M. A.; Emge, T. J.; Wang, H. H.; Carlson, K. D.; Crabtree, G. W. *J. Am. Chem. Soc.* **1985**, *107*, 5815. (b) Clementi, E.; Roetti, C. *At. Nucl. Data Tables* **1974**, *14*, 177.
(20) Bondi, A. *J. Chem. Phys.* **1964**, *68*, 441.
(21) Torrance, J. B.; Scott, B. A.; Walter, B; Kaufman, F. B.; Seiden, P. E. *Phys. Rev.* **1979**, *B19*, 730.

Table 2. Crystallographic Data for BET-TTF Derived Salts

	$(BET\text{-}TTF)_2PF_6$	$(BET\text{-}TTF)_2AsF_6$	$(BET\text{-}TTF)_2SbF_6$	$(BET\text{-}TTF)PF_6$
chem formula	$C_{20}H_{16}S_{12}PF_6$	$C_{20}H_{16}S_{12}AsF_6$	$C_{20}H_{16}S_{12}SbF_6$	$C_{10}H_8S_6PF_6$
formula wt	786.12	830.03	876.85	465.52
dimensions (mm)	not measured	1.01 × 0.54 × 0.005	0.60 × 0.56 × 0.01	0.34 × 0.22 × 0.01
shape	plates	plates	plates	plates
color	black	brown	brown	brown
space group	$P-1$	$P-1$	$P-1$	$P21/a$
Z	1	1	1	2
a (Å)	6.282(2)	6.296(7)	6.289(4)	10.87(1)
b (Å)	7.178(3)	7.20(1)	7.223(4)	4.170(1)
c (Å)	15.69(3)	15.92(3)	16.05(1)	17.15(2)
α (deg)	79.77(7)	79.18(9)	79.43(5)	90.0
β (deg)	82.22(6)	81.79(8)	81.44(4)	99.8(5)
γ (deg)	82.16(3)	82.10(8)	82.18(5)	90.0
V (Å^3)	685(10)	697(2)	704.5(8)	766(1)
D_{calc} (g cm^{-3})	1.91	1.98	2.07	2.02
μ (cm^{-1})	10.32	20.81	18.45	9.53
intervals h,k,l		±8, ±9, 0−19	±7, ±8, 0−19	±12, 0−4, 0−20
collected reflns		2559	2613	1592
unique reflns		2355	2483	1340
used reflns		1372 [$F > 4\sigma(F)$]	2460 [$F > 5\sigma(F)$]	632 [$F > 5\sigma(F)$]
$R(F)$		10.87	5.57	10.13
$wR(F)$		10.87	6.15	10.97

[a] For the $(BETTTF)_2PF_6$ salt only the cell parameters were measured.

despite their different counterions. The B band, due to the presence of doubly charged sites, appears also at the same frequency for all compounds. This situation, which appears in other BET-TTF salts with 2:1 stoichiometry,[8d,22] has also been described for dimethylethylenedithiotetrathiafulvalene (DIMET) 2:1 salts with octahedral anions and $(BEDT)_2\ ICl_2$.[23] In accordance with its completely ionic character, $(BET\text{-}TTF)PF_6$ (**2**) presents only an intense B band.

Transport Properties. As shown in Figure 7 and Table 5 the three $(BET\text{-}TTF)_2X$ salts exhibit high room-temperature conductivities and metallic behaviors. Their single-crystal electrical conductivities at ambient pressure and room temperature are of the same order of magnitude. When the temperature is decreased, an activated behavior appears and a broad minimum in resistivity is observed around 100 K. Although the salt with the bigger anion has the higher transition temperature, it is not possible to establish a clear correlation between the anion size and the T_{M-I}. Because of the thinness of the crystals and also due to the disorder in the structure there is a large standard deviation of the T_{M-I} values (Table 5). The broad minima observed in all measured samples suggest a metal-to-insulator transition induced by an electron localization that could be a consequence of orientational disorder effects.

It is noteworthy that the fully transferred salt $(BET\text{-}TTF)PF_6$ has a high room-temperature conductivity, 10 S cm^{-1}. This fact can be explained by a small on-site Coulomb repulsion U that is in accordance with both the small difference between the first and the second ionization potential of BET-TTF[7c] and the high interstacks conectivity through S···S contacts in the crystal packing.

Thermoelectric power measurements of mixed valence salts (Figure 8) confirm the metallic properties at high temperatures for the three $(BET\text{-}TTF)_2X$ salts. As expected, from the positive values of relative thermopower, it is realized that the charge carriers for these three salts are all holes. The thermopower values start to deviate from the linear curve at temperatures (T_{break}) that are in agreement with the conductivity data; i.e., all values of T_{break} (Table 5) fall into the range of T_{M-I}, respectively. In all cases below the M−I transition, the thermopower first decreases quickly to a minimum and then increases toward larger positive values upon cooling. This indicates a semiconducting behavior in agreement with the resistivity data previously mentioned.

ESR Measurements. The room-temperature ESR line shapes for salts **1**−**5** are Lorentzian for all positions of the crystals with respect to the static magnetic field. The room-temperature line widths are anisotropic with values for the mixed valence salts **1** and **3**−**5** which vary from 8 to 14 G, whereas those for the completely transferred salt **2** are twice larger; i.e., between 18 and 29 G. This behavior is in accordance with the β-like and α-like crystal packing motifs of 2:1 and 1:1 salts, respectively. Although the origin of the ESR line widths for organic metals is not clearly understood, the contribution from spin−orbit coupling certainly plays a major role. This coupling is predominantly influenced by the surrounding symmetry of each BET-TTF radical cation in the solid. If we follow the rationale applied for BEDT-TTF salts,[24] in which it has been considered that the interstack spin−orbit scattering is more effective in the α-phase materials that in the β-phase ones, and if we take into account the modified Elliot formula, first developed for $(TMTSF)_2X$ salts,[25] the resulting line widths of α-phases (W-type interstack packing modes) will be broader than those of the β-phases (L-type interstack packing motifs). In all BET-TTF salts, the minimum g values are very close to the free-electron g value and are found when the static magnetic field is parallel to the stacking axis (crystallographic b axis). This result is expected when the magnetic field is applied normal to planar molecular radicals and is similar to that previously observed for TTF and BEDT-

(22) Rovira, C.; et al., unpublished results.
(23) Garrigou-Lagrange, Ch.; Dupart, E.; Morand, J. P.; Delhaes, P. *Synth. Met.* **1988**, *27*, B537.
(24) Reference 1b, p 190.
(25) Forró, L.; Sckretarczyk, G.; Krupsky, M.; Schweitzer, D.; Keller, H. J. *Phys. Rev. B* **1987**, *35*, 2501.

Table 3. Atomic Coordinates, Equivalent Isotropic Thermal Parameters,[a] and Occupation Factors of BET-TTF Derived Salts

$(BET\text{-}TTF)_2SbF_6$	X/A	Y/B	Z/C	B_{eq}	S_{of}
Sb	0.5000(0)	0.0000(0)	0.0000(0)	2.63	0.5
F1	0.2168(9)	0.1164(10)	0.0051(4)	6.89	1.0
F2	0.4866(9)	−0.0473(9)	−0.1093(3)	5.95	1.0
F3	0.6010(12)	0.2318(9)	−0.0448(5)	8.48	1.0
S1	0.1801(2)	0.3053(2)	0.3268(1)	2.43	1.0
S2	−0.2922(2)	0.3569(2)	0.3784(1)	2.47	1.0
S3	−0.3641(5)	0.4591(6)	0.1901(1)	3.29	0.8
S4	0.2555(2)	0.1981(2)	0.5251(1)	2.57	1.0
S4′	0.1209(8)	0.3963(24)	0.1393(3)	2.46	0.2
S5	−0.2174(2)	0.2513(2)	0.5759(1)	2.49	1.0
S6	0.3217(5)	0.0920(4)	0.7145(1)	2.68	0.8
S9′	−0.1670(8)	0.1583(30)	0.7628(3)	3.33	0.2
C1	−0.0340(4)	0.3004(7)	0.4092(2)	2.12	1.0
C2	0.0138(5)	0.3665(8)	0.2464(2)	2.33	1.0
C3	−0.1988(5)	0.3896(8)	0.2702(2)	2.39	1.0
C3′	−0.3127(18)	0.4412(104)	0.1916(3)	5.39	0.2
C4	0.0738(10)	0.4058(24)	0.1510(3)	3.75	0.8
C5	−0.1414(6)	0.4320(11)	0.1127(3)	3.81	1.0
C6	−0.0029(4)	0.2552(8)	0.4940(2)	2.16	1.0
C6′	0.2699(11)	0.1156(100)	0.7127(2)	4.63	0.2
C7	0.1599(5)	0.1615(7)	0.6330(2)	2.19	1.0
C8	−0.0530(5)	0.1854(7)	0.6566(2)	2.23	1.0
C9	−0.1205(9)	0.1451(17)	0.7514(3)	2.31	0.8
C10	0.0940(6)	0.1070(10)	0.7908(3)	3.42	1.0

$(BET\text{-}TTF)_2AsF_6$	X/A	Y/B	Z/C	B_{eq}	S_{of}
As	0.5000(0)	0.0000(0)	0.0000(0)	4.05	0.5
F1	0.2359(23)	0.0854(26)	0.0045(11)	7.41	1.0
F2	0.5157(29)	0.0395(27)	0.0994(11)	8.22	1.0
F3	0.5616(30)	0.2214(28)	−0.0314(12)	9.30	1.0
S1	0.1793(7)	0.3044(9)	0.3251(3)	2.74	1.0
S2	−0.2921(7)	0.3516(9)	0.3762(3)	2.64	1.0
S3	−0.3659(17)	0.4479(17)	0.1869(5)	3.60	0.7
S4	0.2554(8)	0.2005(10)	0.5254(4)	3.01	1.0
S4′	0.1141(25)	0.3844(46)	0.1364(9)	3.70	0.3
S5	−0.2168(8)	0.2500(9)	0.5755(3)	2.76	1.0
S6	0.3238(14)	0.0997(13)	0.7170(4)	2.17	0.7
S9′	−0.1522(24)	0.1385(40)	0.7615(9)	3.53	0.3
C1	−0.0358(31)	0.2992(32)	0.4084(14)	2.54	1.0
C2	0.0096(29)	0.3629(32)	0.2437(9)	2.62	1.0
C3	−0.1984(27)	0.3849(29)	0.2674(10)	2.19	1.0
C3′	−0.3087(26)	0.4791(24)	0.1864(7)	7.23	0.3
C4	0.0738(30)	0.4122(61)	0.1451(9)	2.25	0.7
C5	−0.1453(20)	0.4322(45)	0.1086(10)	4.37	1.0
C6	−0.0056(25)	0.2547(30)	0.4946(13)	2.41	1.0
C6¢	0.2676(22)	0.0684(22)	0.7165(7)	3.83	0.3
C7	0.1612(26)	0.1652(33)	0.6349(9)	2.44	1.0
C8	−0.0473(29)	0.1872(29)	0.6548(9)	2.08	1.0
C9	−0.1089(34)	0.1809(72)	0.7530(9)	5.28	0.7
C10	0.1013(19)	0.1067(36)	0.7948(9)	3.46	1.0

(BET-TTF)PF6	X/A	Y/B	Z/C	B_{eq}	S_{of}
P	0.2534(19)	−0.1212(32)	0.0034(13)	12.40	0.5
F1	0.2870(20)	0.1532(32)	0.0824(12)	14.64	1.0
F2	0.3102(23)	0.0830(37)	−0.0434(16)	19.15	1.0
F3	0.1197(20)	0.1505(36)	−0.0105(14)	19.17	1.0
S1	−0.1038(3)	−0.1592(9)	0.3855(2)	2.97	1.0
S2	0.1394(3)	0.1778(9)	0.4313(2)	3.05	1.0
S3	0.1774(4)	0.1430(10)	0.2571(2)	3.80	1.0
C1	0.0094(12)	0.0082(27)	0.4627(6)	2.24	1.0
C2	−0.0175(12)	−0.0790(25)	0.3125(7)	2.39	1.0
C3	0.0943(13)	0.0622(26)	0.3340(7)	2.64	1.0
C4	−0.0569(13)	−0.1600(27)	0.2235(6)	3.05	1.0
C5	0.0563(15)	−0.0178(34)	0.1852(9)	5.19	1.0

[a] $B_{eq} = {}^4/_3(a^2B_{11} + b^2B_{22} + c^2B_{33} + ab\cos\gamma\, B_{12} + ac\cos\beta\, B_{13} + bc\cos\alpha\, B_{23})$.

TTF charge-transfer salts.[26] The average g factor values for the different salts are almost the same as those observed for free BET-TTF ions in solution.[7c] Very similar EPR parameters (g values and line widths) are found for isostructural $(BET\text{-}TTF)_2X$ salts despite their different anion components. By contrast and as expected by comparison with the BEDT-TTF salts,[1b] different phases of PF_6 salts show different ESR parameters (Table 6). The same similarities and discordances had been found in the variation of ESR parameters with temperature. Variable-temperature ESR measurements were performed on all salts from 300 to 140 K and on **3**−**5** from 300 to 4.2 K. In all salts g values are temperature independent. As exemplified in Figure 5 for $(BET\text{-}TTF)_2AsF_6$, for isostructural 2:1 salts, the line width decreases monotonically with decreasing temperature in all temperature ranges, which is a common behavior in many organic metals,[21,27] and can be attributed to temperature-dependent scattering processes since, as mentioned above, the ESR line width might be described by the modified Elliot formula for the spin relaxation in metals.[25] The spin susceptibility decreases smoothly with decreasing temperature. This behavior is observed in many highly conducting organics with an essentially one-dimensional (1D) gas flow.[28] From the above-mentioned ESR characteristics of $(BET\text{-}TTF)_2X$ salts, a phase transition is not observed, which is in agreement with a electron localization promoted metal−semiconductor transition also suggested from the conductivity measurements. In fact, The data of χ vs T of these salts is very similar to that observed for $(TMTTF)_2X$ series, which undergoes a Mott−Hubbard localization at low temperatures.[29] To study if the insulating ground state is an antiferromagnetic ground state, ESR studies at lower temperatures are required. The absence of an structural change associated with the metal-to-insulator transition has also been confirmed by IR spectroscopy because no change was observed in the IR spectra at 300 and 15 K.

Indeed, the ESR characteristics of the mixed valence solvate $(BET\text{-}TTF)_3PF_6{\cdot}C_6H_5Cl$ (**1**) are very analogous to those of the above-explained 2:1 salts. This fact and the similarity found in the UV−NIR spectra suggest that the crystal packing of donors in salt **1** is very similar to that of salts **3**−**5**. By contrast and in accordance with its completely ionic character, the semiconducting salt $(BET\text{-}TTF)PF_6$ presents a completely different behavior of its ESR parameters with temperature. The line width decreases more strongly and the spin susceptibility follows a Curie law characteristic of a highly localized noninteracting spins system.

Electronic Band Structure. The structural and physical studies of the 2:1 BET-TTF salts reported above lead to two somewhat puzzling observations. First, although from the structural viewpoint they are very similar to the β-type salts of BEDT-TTF, which are usually two-dimensional (2D) metals, the ESR results rather suggest 1D type behavior. Second, despite the existence of a quite noticeable orientational disorder, the salts are metallic until relatively low temperatures. This brings to the fore two important issues. Because of the nature of the BET-TTF molecule, the orienta-

(26) (a) Wudl, F.; Schafer, D. E.; Walsh, W. M.; Rupp, L. W.; DiSalvo, F. J.; Waszczak, J. V.; Kaplan, M. L.; Thomas, G. A. *J. Chem. Phys.* **1977**, *66*, 377. (b) Sugano, T.; Saito, G.; Kinoshita, M. *Phys. Rev. B* **1986**, *34*, 117. (c) Enoki, T.; Imaeda, K.; Kobayashi, M.; Inokuchi, H.; Saito, G. *Phys. Rev. B.* **1986**, *33*, 1553. (d) Scott., J. C. In *Highly Conducting Quasi-One-Dimensional Organic Crystals*; Conwell, E., Ed.; Academic Press: San Diego, CA, 1988; p 390.

(27) Scott, J. C. In ref 26d, p 404.

(28) Pedersen, H. J.; Scott, J. C.; Bechgaard, K. *Solid St. Commun.* **1980**, *35*, 207.

(29) (a) Laversanne, R., Coulon, C.; Gallois, B.; Pouget, J. P. Moret, R. *J. Phys. Lett.* **1984**, *45*, 393. (b) Coulon C. In *Organic and Inorganic Low Dimensional Crystalline Materials;* Delhaes, P., Drillon, M., Eds.; NATO ASI Series; Plenum Press: New York, 1987; p 201.

Table 4. Bond Lengths and Angles for BET-TTF Derived Salts

$(BET\text{-}TTF)_2SbF_6$

Bond Distances (Å)

F1–Sb	1.855(5)	C6–S4	1.741(2)	C4–C2	1.504(3)
F3–Sb	1.855(5)	C2–S4′	1.734(3)	C3–C2	1.329(3)
F2–Sb	1.864(4)	C5–S4′	1.735(3)	C3′–C3	1.504(3)
C1–S1	1.739(2)	C8–S5	1.732(2)	C5–C3′	1.540(3)
C2–S1	1.735(2)	C6–S5	1.735(2)	C5–C4	1.540(3)
C3–S2	1.731(2)	C7–S6	1.733(2)	C10–C6′	1.541(3)
C1–S2	1.738(2)	C10–S6	1.744(3)	C7–C6′	1.504(3)
C3–S3	1.730(2)	C10–S9′	1.735(3)	C7–C8	1.330(3)
C5–S3	1.743(3)	C8–S9′	1.735(3)	C8–C9	1.503(3)
C7–S4	1.730(2)	C6–C1	1.375(5)	C9–C10	1.541(3)

Bond Angles (deg)

F1–Sb–F2	90.4(2)	C4–C2–C3	113.2(3)	S4–C6–C1	121.6(2)
F2–Sb–F3	91.2(3)	S1–C2–C3	117.2(2)	C7–C6′–C10	108.4(4)
F1–Sb–F3	90.1(3)	S1–C2–C4	129.5(3)	S4–C7–C6′	133.2(3)
C1–S1–C2	94.3(2)	S4′–C2–C3	121.5(3)	C8–C7–C6′	108.0(3)
C1–S2–C3	93.9(2)	S2–C3–C3′	132.7(4)	S4–C7–C8	118.7(2)
C3–S3–C5	90.6(2)	C2–C3–C3′	108.8(4)	S4–C7–S6	124.8(2)
C6–S4–C7	93.6(1)	S2–C3–C2	118.5(2)	C8–C7–S6	116.5(2)
C2–S4′-C5	88.8(3)	S2–C3–S3	124.2(2)	S5–C8–C9	128.1(2)
C6–S5–C8	94.3(2)	C2–C3–S3	117.2(2)	C7–C8–C9	114.8(3)
C7–S66–C10	90.5(2)	C3–C3′–C5	108.3(4)	S5–C8–C7	117.2(2)
C8–S9′-C10	87.9(3)	C2–C4–C5	105.8(4)	S5–C8–S9′	120.1(2)
S1–C1–S2	116.0(2)	S4′–C5–C3′	112.1(5)	C7–C8–S9′	122.8(3)
S2–C1–C6	121.5(2)	C4–C5–S3	111.5(4)	C8–C9–C10	104.7(4)
S1–C1–C6	122.5(2)	S4–C6–S5	116.2(2)	C6′–C10–S9′	112.9(4)
S1–C2–S4′	121.3(2)	S5–C6–C1	122.2(2)	S6–C10–C9	112.9(4)

$(BET\text{-}TTF)_2AsF_6$

Bond Distances (Å)

F1–As	1.69(1)	C7–S4	1.74(2)	C3′–C3	1.550(3)
F2–As	1.68(2)	C5–S4′	1.726(9)	C2–C3	1.31(2)
F3–As	1.66(2)	C2–S4′	1.726(9)	C5–C3′	1.550(3)
C2–S1	1.75(2)	C6–S5	1.71(2)	C5–C4	1.551(3)
C1–S1	1.75(2)	C8–S5	1.73(2)	C2–C4	1.550(3)
C1–S2	1.73(2)	C10–S6	1.735(9)	C6′–C7	1.550(3)
C3–S2	1.73(2)	C7–S6	1.731(8)	C9–C8	1.550(3)
C3–S3	1.731(8)	C8–S9′	1.721(9)	C7–C8	1.30(2)
C5–S3	1.735(9)	C10–S9′	1.726(9)	C9–C10	1.550(3)
C6–S4	1.75(2)	C6–C1	1.38(3)	C6′–C10	1.550(3)

Bond Angles (deg)

F1–As–F2	92.5(8)	C3–C2–S4′	122(1)	C1–C6–S4	121(1)
F3–As–F2	84.5(9)	C3–C2–C4	114(1)	C10–C6′–C7	107(1)
F1–As–F3	88.9(9)	C3–C2–S1	117(1)	C8–C7–S4	116.4(9)
C2–S1–C1	93.7(8)	C4–C2–S1	128(1)	S6–C7–S4	125(1)
C3–S2–C1	94.1(8)	C2–C3–S2	119.0(9)	C6′–C7–S4	133(1)
C5–S3–C3	90.7(9)	C3′–C3–C2	107(1)	S6–C7–C8	119(1)
C7–S4–C6	93.2(8)	C3′–C3–S2	132(1)	C6′–C7–C8	109(1)
C5–S4′–C2	89(1)	S3–C3–S2	124(1)	S9′–C8–S5	120(1)
C8–S5–C6	92.7(8)	S3–C3–C2	117(1)	C7–C8–S9′	119(1)
C10–S6–C7	91.6(8)	C5–C3′–C3	105(1)	C9–C8–C7	111(1)
C10–S9′–C8	92(1)	C5–C4–C2	103(1)	C7–C8–S5	121(1)
C6–C1–S2	121(1)	C3′–C5–S4′	111(1)	C9–C8–S5	127(1)
S1–C1–S2	116(1)	S3–C5–C4	113(1)	C10–C9–C8	106(1)
C6–C1–S1	123(1)	C1–C6–S5	122(1)	C9–C10–S6	111(1)
S4′–C2–S1	121(1)	S5–C6–S4	117(1)	C6′–C10–S9′	107(1)

$(BET\text{-}TTF)PF_6$

Bond Distances (Å)

P–F1	1.764(22)	C1–S2	1.744(13)	C1*–C1	1.332(21)
P–F3	1.825(24)	C3–S2	1.727(11)	C3–C2	1.345(18)
P–F2	1.386(26)	C5–S3	1.775(15)	C4–C2	1.551(15)
C2–S1	1.719(13)	C3–S3	1.752(13)	C5–C4	1.603(19)
C1–S1	1.789(12)				

Bond Angles (deg)

F1–P–F2	90(1)	S1–C1–S2	114.9(6)	C2–C3–S3	115.8(9)
F1–P–F3	76(1)	C1*–C1–S2	126(1)	S2–C3–C2	119(1)
F2–P–F3	88(1)	C1*–C1–S1	120(1)	S2–C3–S3	125.2(8)
C1–S1–C2	94.1(5)	S1–C2–C3	117.7(9)	C2–C4–C5	103(1)
C1–S2–C33	94.2(6)	C3–C2–C4	117(1)	C4–C5–S3	113(1)
C3–S3–C5	92.0(6)	S1–C2–C4	126(1)		

tional disorder directly affects the number of S···S intermolecular contacts. Thus, the question arises of how this orientational disorder can affect the electronic band structure and the Fermi surface of these (and other) β-type BET-TTF salts. Also, if the metal-to-insulator transition is driven by a localization phenom-

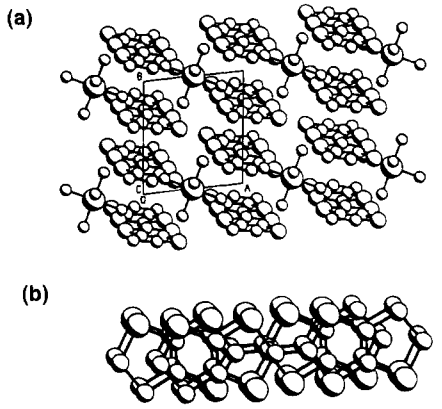

Figure 2. (a) X-ray crystal packing of $(BET\text{-}TTF)_2SbF_6$ (**5**), projection along *c*. (b) Overlap mode of BET-TTF molecules in **5**, view perpendicular to the molecular plane 1.

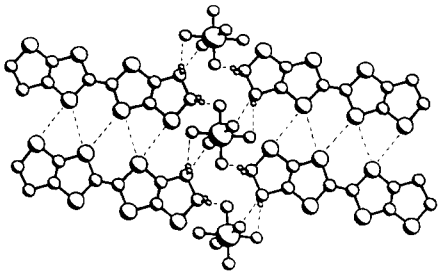

Figure 3. Projection in the *a*−*c* plane of the structure of $(BET\text{-}TTF)_2SbF_6$ (**5**) showing close intermolecular contacts, (S···S < 3.68 Å; F···H < 2.55 Å).

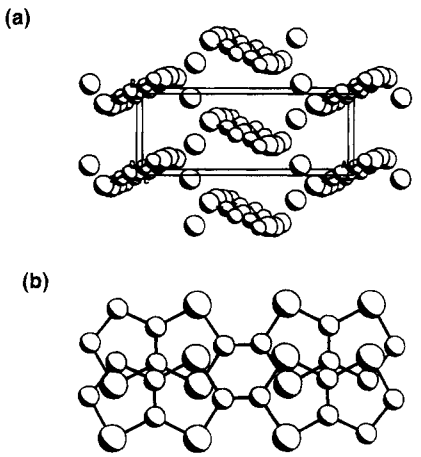

Figure 4. (a) X-ray crystal packing of $(BET\text{-}TTF)PF_6$ (**2**), projection along *c*. F atoms were omitted for clarity. P atoms are disorderes, with an occupation factor of 0.50. (b) Overlap mode of BET-TTF molecules in **2**, view perpendicular to the molecular plane 1.

enon (a question which we should look at more carefully) and could be suppressed by an applied pressure, is there any chance for these salts to retain their metallic behavior until very low temperatures? If yes, since the β-type structure seems to sustain superconductivity in a number of BEDT-TTF salts, it would be likely that the present BET-TTF salts could be superconducting under pressure. To discuss some of these aspects, we carried out a tight-binding extended Hückel band structure study of the donor slabs of the $(BET\text{-}TTF)_2X$ (X = SbF_6 and AsF_6).

To begin with, let us consider an ordered slab where all BET-TTF donors have the predominant orientation found in the structure of the $(BET\text{-}TTF)_2SbF_6$ salt.

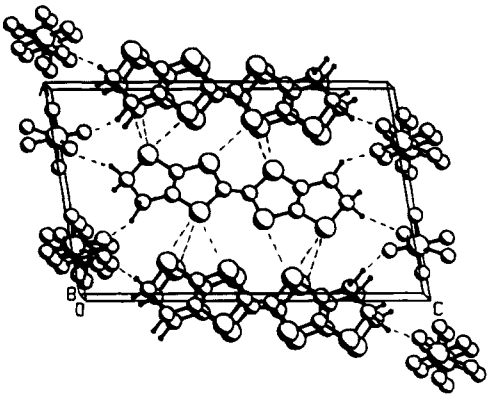

Figure 5. Projection in the *a*−*c* plane of the structure of $(BET\text{-}TTF)PF_6$ (**2**) showing close intermolecular contacts (S···S < 3.68 Å; F···H < 2.55 Å).

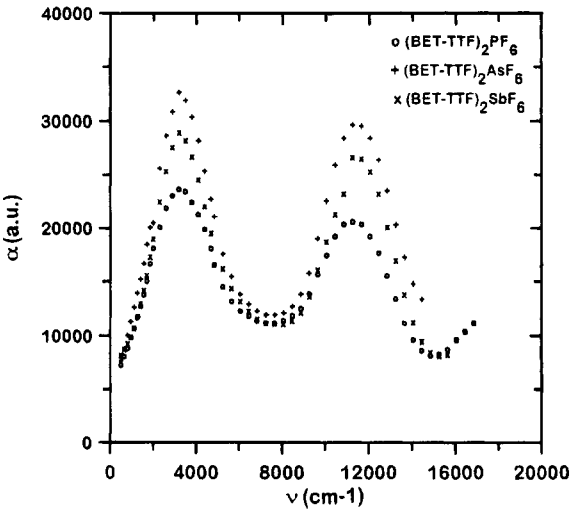

Figure 6. Mean electronic absorption coefficient α versus energy of $(BET\text{-}TTF)_2X$ salts **3**−**5**.

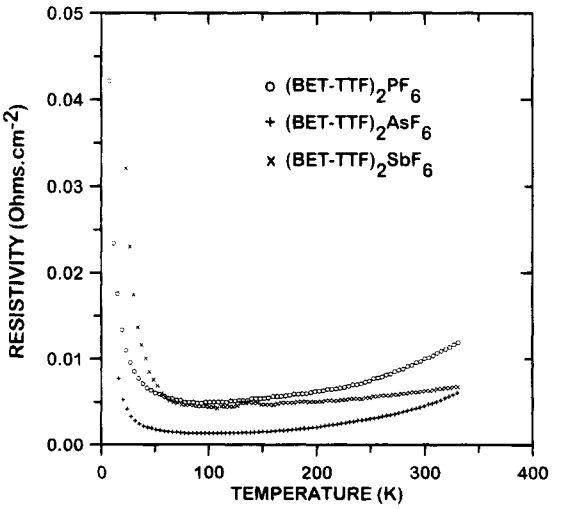

Figure 7. Temperature dependence of a representative crystal resistivities of $(BET\text{-}TTF)_2X$ salts **3**−**5**.

Taking into account all S···S contacts smaller than 4.0 Å, there are five different types of donor···donor intermolecular interactions. These interactions are schematically shown in **6**, which is a view perpendicular to the slab and where every donor is represented by a straight line. The absolute values of the $\beta_{HOMO-HOMO}$ interaction energies for these intermolecular interactions as well as the associated S···S distances are

Table 5. Conductivity and Thermopower Data

	compound			
	BET-TTFPF$_6$ (**2**)	(BET-TTF)$_2$PF$_6$ (**3**)	(BET-TTF)$_2$AsF$_6$ (**4**)	(BET-TTF)$_2$SbF$_6$ (**5**)
σ_{300} (S/cm)[a]	10	117	220	160
σ_{max} (S/cm)[a]		240	900	300
$\sigma_{max}/\sigma_{300}$		2.4	4.1	1.8
$T_{transition}$ (K)[b]		75–102	84–120	125–145
T_{break} (K)[c]		125	100	122

[a] Average value of four samples. [b] Temperature at which resistivity values are minimum. [c] Temperature at which thermopower values start to deviate from the linear curve in the high-temperature ranges.

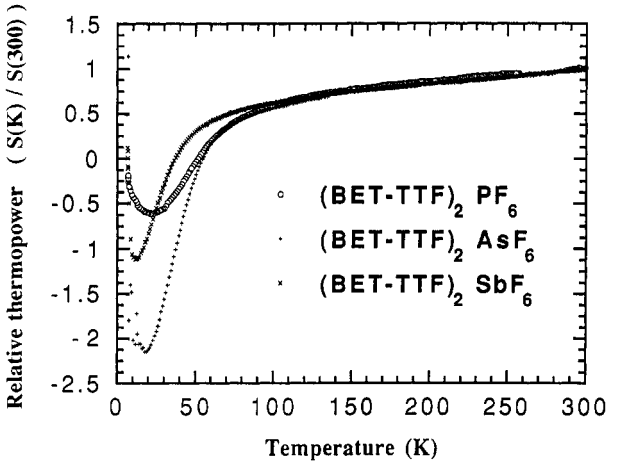

Figure 8. Temperature dependence of relative thermopower of (BET-TTF)$_2$X salts **3**–**5**.

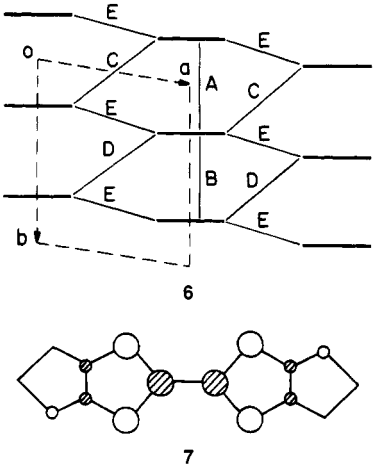

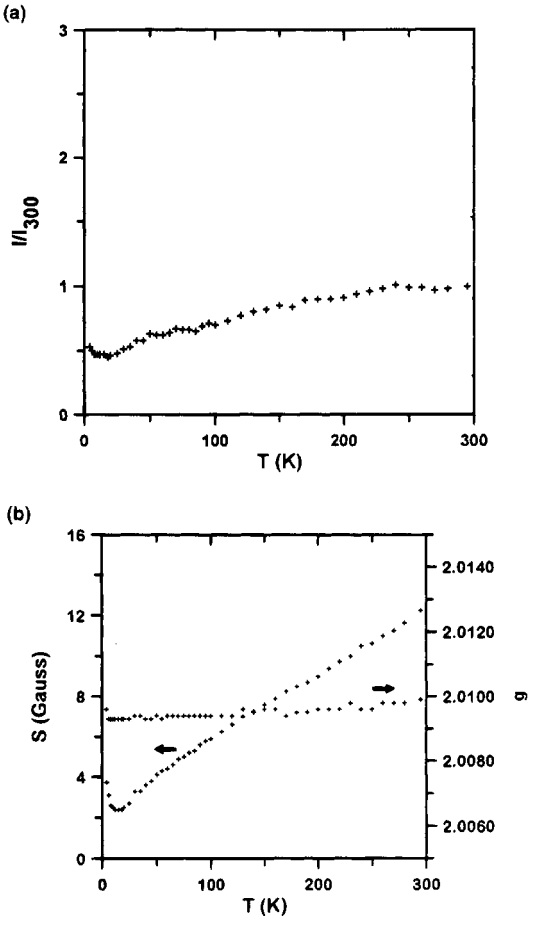

Figure 9. Temperature dependence of the (a) normalized spin susceptibility, (b) line width, and g value of a single crystal of (BET-TTF)$_2$ASF$_6$ (**4**).

reported in Table 7. The interaction energies are a measure of the strength of the interaction between a pair of BET-TTF HOMOs in adjacent sites of the crystal and give important insight concerning the correlation between the crystal and electronic structures of molecular solids.[30] The interaction energies for the two intermolecular contacts along the zigzag chains (A and B) are quite similar and between 3 and 5 times larger than those for the interchain intermolecular interactions (C, D, and E). These interaction energies are quite comparable to those reported for β-(BEDT-TTF)$_2$I$_3$[30a] and denote a considerable degree of two-dimensionality. It is worthwhile noting that many of the S···S distances of Table 7 are quite long and yet lead to very sizable interaction energies.

The calculated band structure for the donor slabs of (BET-TTF)$_2$SbF$_6$ assuming no disorder is shown in Figure 10. The repeat unit of the slab contains two donor molecules, and thus there are two HOMO bands. The total width of these HOMO bands is quite large and the dimerization gap (i.e., the energy gap at Y) only modest. The individual dispersions along the interchain direction (i.e., $\Gamma \rightarrow X$) are about half those along the chain direction (i.e., $\Gamma \rightarrow Y$). Thus, the ordered donor slabs of (BET-TTF)$_2$SbF$_6$ can be seen as a series of relatively strongly interacting quite uniform zigzag chains. With the formal oxidation state required by the stoichiometry, (BEDT-TTF)$_2^+$, there are three electrons to fill these two bands and thus the upper band is half-filled. The Fermi level (dashed line in Figure 10) cuts the band along b^* but lies immediately below the lower

(30) (a) Whangbo, M.-H.; Williams, J. M.; Leung, P. C. W.; Beno, M. A.; Emge, T. J.; Wang, H. H. *Inorg. Chem.* **1985**, *24*, 3500. (b) Williams, J. M.; Wang, H. H.; Emge, T. J.; Geiser, U.; Beno, M. A.; Leung, P. C. W.; Carlson, K. D.; Thorn, R. J.; Schultz, A. J.; Whangbo, M.-H. *Prog. Inorg. Chem.* **1987**, *35*, 51. (c) Since overlap is explicitly included in extended Hückel calculations, these interaction energies (β) should not be confused with the conventional transfer integrals (t). Although the two quantities are obviously related and have the same physical meaning, the absolute values of β are somewhat greater than those of t.

Table 6. Principal g Values[a] and the Corresponding Line Widths (ΔH)[b] at Room Temperature

	compound			
	BET-TTFPF$_6$ (**2**)	(BET-TTF)$_2$PF$_6$ (**3**)	(BET-TTF)$_2$AsF$_6$ (**4**)	(BET-TTF)$_2$SbF$_6$ (**5**)
g_a (ΔH, G)	2.0051 (22)	2.0078 (12)	2.0079 (10)	2.0074 (13)
g_b (ΔH, G)	2.0018 (18)	2.0026 (9)	2.0021 (8)	2.0024 (9)
g_c (ΔH, G)	2.0100 (29)	2.0080 (14)	2.0095 (14)	2.0091 (14)

[a] g_a, g_b, and g_c, correspond to the values when the external magnetic field parallel to a, b, and c crystallographic axis, respectively. [b] ESR peak-to-peak line width.

Table 7. S···S Distances Shorter Than 4.0 Å and Absolute Values of the $\beta_{HOMO-HOMO}$ Interaction Energies (eV) for the Different Donor···Donor Interactions in (BET-TTF)$_2$SbF$_6$ (See 6 for Labeling)

interaction type	S···S distances (Å)	$\beta_{HOMO-HOMO}$
A	3.860 (×2), 3.861 (×2), 3.888 (×2), 3.972 (×2), 3.997 (×2)	0.380
B	3.845 (×2), 3.940 (×2), 3.982 (×2)	0.307
C	3.972 (×2)	0.111
D	(4.008, 4.020)[a]	0.078
E	3.515, 3.566, 3.583, 3.618	0.066

[a] Shortest S···S distances for this interaction.

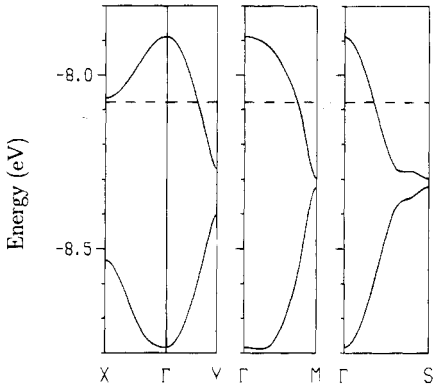

Figure 10. Dispersion relations for the HOMO bands of the ordered donor slabs in (BET-TTF)$_2$SbF$_6$. The dashed line refers to the Fermi level. Γ, X, Y, M, and S are the wave vectors (0, 0), (a*/2, 0), (0, b*/2), (a*/2, b*/2), and (−a*/2, b*/2), respectively.

part of the band along a*. Thus, the calculated Fermi surface, shown in Figure 11, is open along the interchain direction. However, although strictly speaking the presence of two open lines in this Fermi surface indicates a pseudo-1D system,[31] the warping of these lines is very strong and makes clear that there is a strong coupling between these chains. In fact, as can be seen in Figure 10, a small shift of the Fermi level will make it to cross the upper band near X. The resulting Fermi surface would be closed and very similar to that of the β-(BEDT-TTF)$_2$I$_3$ salt.[32] In short, we can conclude that these slabs lie at the boundary between the 1D and 2D systems, which solves the apparent contradiction noted at the beginning of this section.

Let us now turn to the possible effect of the orientational disorder. Because of the sites of the sulfur atoms in the outer five-membered rings, the orientational disorder could change the strength of some of the intermolecular interactions. The simplest way to tackle this problem is to repeat the calculation with the outer five-membered rings replaced by two hydrogen atoms and keeping all geometric details for the remaining part

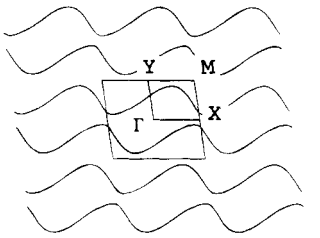

Figure 11. Calculated Fermi surface for (BET-TTF)$_2$SbF$_6$.

of the slab (i.e., using TTF molecules with the same inner core than the BET-TTF ones). The replacement reduces slightly the bandwidths but leaves the Fermi surface practically unaltered. In both band structure and Fermi surface the results for the donor slabs of the SbF_6 and AsF_6 salts are identical. Thus, orientational disorder in these salts can have an effect in somewhat reducing the absolute value of the conductivity but not in changing the anisotropy. The result can be understood by looking at the HOMO of BET-TTF (**7**). As is the case for BEDT-TTF, the outer sulfur contributions (S_o) to this HOMO are considerably smaller ($\sim$1/3) than those of the inner core sulfur atoms (S_i). Since orientational disorder only affects the outer sulfur atoms and S_i···S_i contacts are associated with all the intermolecular interactions of the slabs, the effect on the intermolecular overlaps is not important. In addition, disorder can have an indirect effect by changing the geometry of some intermolecular interactions. This can affect the inner core S···S contacts and thus lead to changes in the intermolecular overlaps. This is the case in BEDT-TTF salts where the conformational flexibility of the outer six-membered rings can have a nonnegligible effect in the spacing between two nearest-neighbor molecules. However, in the case of BET-TTF, the considerably greater rigidity of the outer five-membered rings should not lead to this type of modification. Thus we conclude that the band structures and Fermi surfaces of β-type salts of BET-TTF are not strongly affected by the existence of orientational disorder.

The Fermi surface of Figure 11 exhibits a nesting vector $q = -0.18a^* + 0.5b^*$ which would allow for the destruction of a considerable portion of the surface. Thus, at least in principle, a low-temperature distortion with this wave vector could occur. However, the nesting is only partial so that large pockets would remain even after the distortion and the transition would be of the metal-to-metal type and not metal-to-insulator, as experimentally observed. This fact and the very gradual nature of the transition completely rule out a Fermi surface instability as a possible source for the low-temperature transition in the present salts. We are left with the conclusion that orientational disorder, although it seems not to have an important influence on the band structure and Fermi surface of the system, has yet an important role in forcing the loss of metallic type conductivity at low temperatures. As shown in Figure

(31) Canadell, E.; Whangbo, M.-H. *Chem. Rev.* **1991**, *91*, 965.
(32) (a) See ref 1b, p 261. (b) Doublet, M. L.; Canadell, E., unpublished results.

10, there is practically no gap between the two HOMO bands. Thus, these salts can be considered to have an effective quarter-empty HOMO band. This relatively low number of holes and the existence of disorder within the donor slabs suggest Anderson localization as a plausible origin for the metal-to-insulator transition. An interesting development of the present work would thus be a systematic study of the synthetic conditions in order to see if it is possible to decrease (or eventually suppress) the disorder and see how the transition temperature is modified. Our results also suggest that if this localization could be suppressed by an applied pressure, the salts would keep, at least partially, the metallic type conductivity until low temperatures. It should also be reminded that the Fermi level of Figure 10 lies extremely close to the minimum along the $\Gamma \rightarrow$ X line. Since pressure should increase the band dispersion, it is quite possible that under pressure the Fermi level would cut the higher band along both the $\Gamma \rightarrow$ X and $\Gamma \rightarrow$ Y lines. Under such circumstances the Fermi surface would close and, as mentioned, be very similar to that of the BEDT-TTF β-type salts. Consequently, the analogy between the superconducting BEDT-TTF β salts and the present ones would be very strong both electronically and structurally. We believe that a pressure study of these BET-TTF salts would be very interesting.

Concluding Remarks

The multisulfur BET-TTF donor forms with octahedral anions radical-ion salts with different stoichiometries. $(BET\text{-}TTF)_2X$ (X = PF_6, AsF_6, SbF_6) salts are isostructural and show a β-type packing motif which is characteristic of many of the ET-based organic superconductors, all sulfur atoms of BET-TTF are involved in the S···S contacts that generate a 2D crystal structure. Due to the greater rigidity of the five-membered external ring with respect to the six-membered ring of BEDT-TTF, in BET-TTF salts there is not disorder associated to the ethylene groups but a disorder is observed due to the position of the external sulfur atoms. Despite this characteristic, the three salts are metallic at room temperature but undergo a metal-to-semiconductor transition at about 100 K. Tight-binding band calculations lead us to conclude that both the band structures and the Fermi surface of these β-type salts of BET-TTF are not strongly affected by the existence of orientational disorder, although this disorder has an important role in forcing the loss of metallic character at low temperatures. The Fermi surface lies at the boundary between 1D and 2D systems which accounts for the 1D characteristic of the ESR parameters variation with the temperature and with the 2D structural character. We believe that if under an applied pressure the metal-to-semiconductor transition could be suppressed, the Fermi surface would close, generating a very strong electronic and structural analogy of these BET-TTF salts with the superconducting BEDT-TTF β salts. We are actually working in the synthesis of BET-TTF salts with smaller anions, which would produce a closer packing of the donors and give rise to 2D band structures.

Acknowledgment. Work at ICMB was supported by a grants from the Programa Nacional de Química Fina, (CIRIT-CICyT) Spain (QFN93-4510-CO1), Comissionat per a Universitats i Recerca, and the Human Capital and Mobility Programm of the UE (ERBCHRX CT93-0271). Research at Hopkins was supported by a grant from the National Science Foundation (DMR-9223481). We gratefully acknowledge fruitful discussions with Dr. P. Delhaes and Dr. Ch. Garrigou-Lagrange and thank them and Dr. J. Amiell of Centre de Rechérche Paul Pascal for optical and low-temperature ESR measurements.

CM950131C